Magnetohydrodynamic Peristaltic Flow of a Pseudoplastic Fluid in a Curved Channel

Saima Noreen[a], Tasawar Hayat[b], and Ahmed Alsaedi[c]

[a] Department of Mathematics, Comsats Institute of Information Technology, Attock 43600, Pakistan
[b] Department of Mathematics, Quaid-I-Azam University 45320, Islamabad 44000, Pakistan
[c] Department of Mathematics, Faculty of Science, King Abdulaziz University, P.O.Box 80257, Jeddah 21589, Saudi Arabia

Reprint requests to S. N.; E-mail: laurel_lichen@yahoo.com

Z. Naturforsch. **68a,** 380 – 390 (2013) / DOI: 10.5560/ZNA.2013-0003
Received June 23, 2012 / revised Dezember 17, 2012 / published online March 6, 2013

A mathematical model is developed to examine the effects of an induced magnetic field on the peristaltic flow in a curved channel. The non-Newtonian pseudoplastic fluid model is used to depict the combined elastic and viscous properties. The analysis has been carried out in the wave frame of reference, long wavelength and low Reynolds scheme are implemented. A series solution is obtained through perturbation analysis. Results for stream function, pressure gradient, magnetic force function, induced magnetic field, and current density are constructed. The effects of significant parameters on the flow quantities are sketched and discussed.

Key words: Curved Channel; Induced Magnetic Field.

1. Introduction

Investigations of peristaltic transport of fluids are interesting and have been a topic of several attempts during the last few decades owing to their applications in chyme movement in gastrointestinal tract, spermatozoa transport in the ductus efferents of male reproductive tract, the movement of ovum in female fallopian tube, vasomotion of blood vessels, movement of food bolus through oesophagus, and many others. After the experimental study of Latham [1], a number of investigations have been presented on peristalsis under different flow geometries, assumptions, and fluid models. Few recent representative studies in this direction are done by Tripathi [2 – 5]; Pandey and Chaube [6]; Pandey and Tripathi [7]; Srinivas and Kothandapani [8]; Abd elmaboud and Mekheimer [9]; Hayat et al. [10, 11]; Mekheimer and Abd elmaboud [12]; Mekheimer et al. [13]; Abd elmaboud and Mekheimer [14]; Gharsseldien et al. [15]; Tripathi and Bég [16]; Tripathi et al. [17 – 19]; Bég [20] and many others.

Magnetohydrodynamic (MHD) peristaltic flow has been also an important area of research for the last few years. The flow effects the field and the field in turn react back to effect the flow. Magnetotherapy, magnetic resonance imaging, and magnetic devices are few applications of magnetic fields in physiology. With such awareness, few researchers studied the influence of an applied magnetic field on the peristaltic motion. For example, Nadeem et al. [21] studied the power law fluid model for blood flow through a tapered artery with a stenosis. In another investigation, Nadeem and Awais [22] have discussed the thin film flow of an MHD Oldroyd 8-constant fluid in a vertical cylinder. Hayat et al. [23 – 25] have analyzed the MHD effects on the peristaltic flows of Jeffrey, Carreau, and fourth grade fluid. The analysis presented in the recent investigations [26 – 32] also examined the peristalsis with an applied magnetic field. In continuation, some advancement is made for the peristaltic activity in the presence of an induced magnetic field. A pioneering work regarding an induced magnetic field was done by Pavlov and Vishnyakov [33]. Afterwards, Mekheimer [34] examined the MHD flow of a couple stress fluid in a symmetric channel with an induced magnetic field. Recently, Hayat et al. [35 – 37] discussed the peristaltic transport of incompressible third order, Carreau, and fourth grade fluids in a symmetric channel under

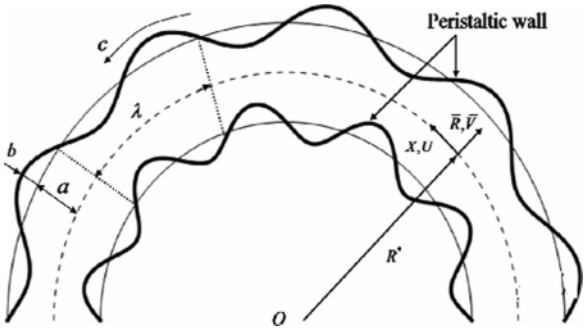

Fig. 1. Geometry of flow problem.

the effects of an induced magnetic field, respectively. In [38], Mekheimer dealt with the flow analysis of an incompressible magneto-micropolar fluid in the presence of an induced magnetic field.

Another important aspect dealing with the peristaltic flow in a curved channel is not given proper attention so far. The literature is repleted with the peristaltic flows in a straight channel. The consideration of a curved channel is important especially for the analysis of peristaltic flows in physiological processes. Mostly, peristalsis is studied in straight channels and tubes. However, the geometry of most physiological conduits and glandular ducts is curved. A model of micro wrinkles on human skin also requires a curved geometry. The geometry of airways and arterial network produces swirling flows, similar to the flows found in curved or twisted pipes. With this motivation, Sato et al. [39] analyzed the peristaltic flow in a curved channel. Ali et al. [40] reconsidered the analysis of [39] in the wave frame of reference. In continuation, Ali et al. [41, 42] discussed the peristaltic transport of third order and micropolar fluid in a curved channel.

The present research has been undertaken to investigate the peristaltic transport of a pseudoplastic fluid in a curved channel. The differential equations are modelled, and the mathematical problem is solved in series form. Special attention in the analysis is given to the induced magnetic field effect. The paper is structured as follows: Section 2 presents the mathematical formulation, Section 3 contains the series solutions, and a discussion is given in Section 4; Section 5 includes concluding remarks.

2. Mathematical Formulation

Consider a curved channel with half width a. The circular shape of the channel has radius R and centre O with the space occupied by an incompressible pseudoplastic fluid. A sinusoidal wave of velocity c propagates on the channel walls. We choose coordinates $(\bar{R}, \bar{X})$ with $\bar{X}$ in the direction of wave propagation and $\bar{R}$ transverse to it as shown in Figure 1. An external magnetic field of strength H_0^* $\left(= H_0 \frac{R^*}{R^* + \bar{R}}\right)$ acts in the radial direction (H_0 is the con-

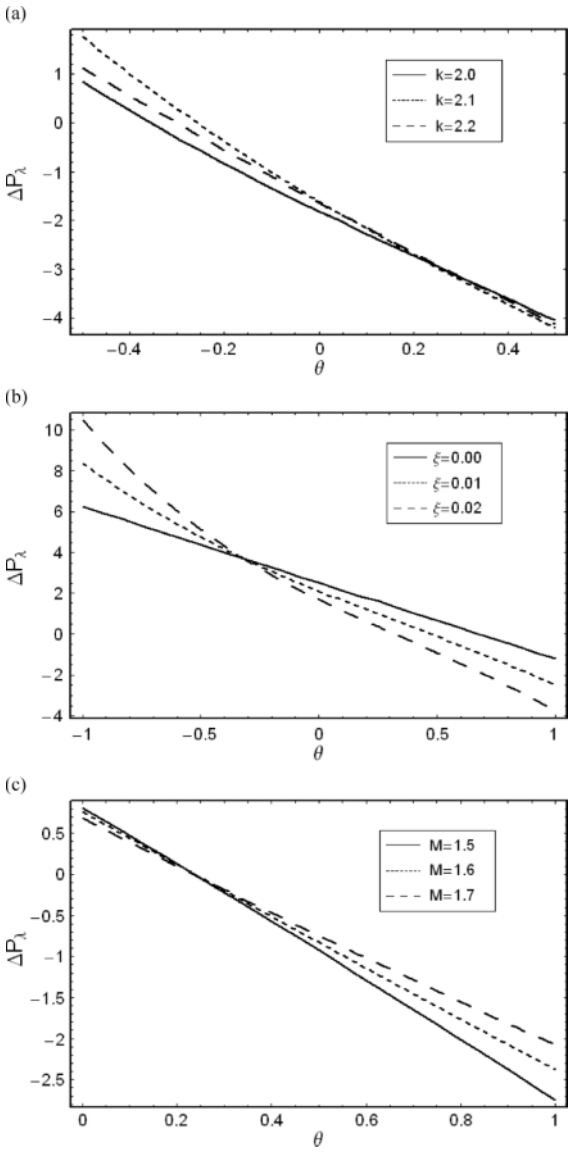

Fig. 2. (a) Pressure rise ΔP_λ versus flow rate θ for $\alpha = 0.4$, $M = 1.4$, $E = 1$, and $\xi = 2$. (b) Pressure rise ΔP_λ versus flow rate θ for $\alpha = 0.4$, $M = 1.4$, $E = 1$, and $k = 2$. (c) Pressure rise ΔP_λ versus flow rate θ for $\alpha = 0.2$, $k = 2.5$, $\xi = 0.01$, and $E = 1.4$.

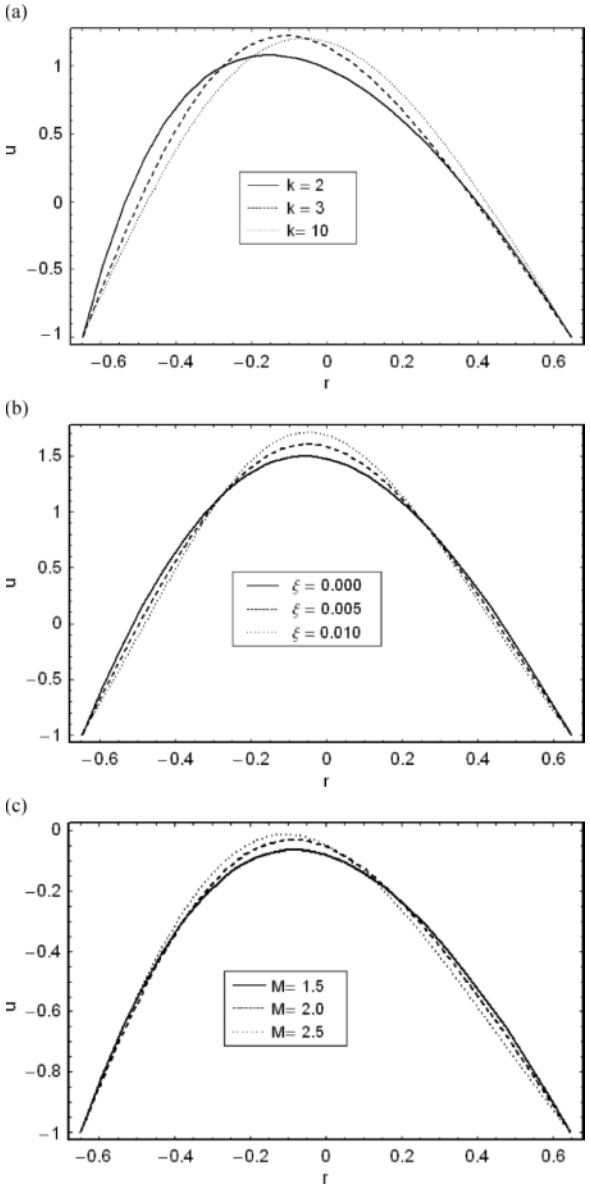

Fig. 3. (a) Axial velocity u versus r for $\xi = 0.01$, $\alpha = 0.6$, $M = 1.9$, $x = 0.6$, and $\theta = 2.5$. (b) Axial velocity u versus r for $k = 3.2$, $\alpha = 0.6$, $M = 1.9$, $x = 0.6$, and $\theta = 2.8$. (c) Axial velocity u versus r for $\xi = 0.01$, $\alpha = 0.6$, $k = 3.2$, $x = 0.6$, and $\theta = 1.5$.

stant magnetic field). This results in an induced magnetic field $H\left(\bar{h}_{\bar{r}}(\bar{R},\bar{X},\bar{t}),\bar{h}_{\bar{x}}(\bar{R},\bar{X},\bar{t}),0\right)$ and therefore the total magnetic field becomes $H^{+}\ (H_0^{*}+\bar{h}_{\bar{r}}(\bar{R},\bar{X},\bar{t}),\bar{h}_{\bar{x}}(\bar{R},\bar{X},\bar{t}),0)$. The wall surface is represented by the following expression:

$$\bar{h}(\bar{X},\bar{t}) = a + b\sin\left(\frac{2\pi}{\lambda}(\bar{X}-c\bar{t})\right). \tag{1}$$

In the above equations, λ is the wavelength, $\bar{t}$ the time, and b the wave amplitude. Indicating the velocity components $\bar{V}$ and $\bar{U}$ along the radial $(\bar{R})$ and axial directions $(\bar{X})$, respectively, in the fixed frame, the velocity field V can be represented in the expression

$$V = [\bar{V}(\bar{R},\bar{X},\bar{t}),\bar{U}(\bar{R},\bar{X},\bar{t}),0]\,. \tag{2}$$

The fundamental equations governing the flow of an incompressible fluid are:

Continuity equation

$$\nabla\cdot V = 0\,. \tag{3}$$

Equation of motion [34]

$$\begin{aligned}\rho\frac{\mathrm{d}V}{\mathrm{d}t} &= \mathrm{div}\bar{\mathbf{T}} + \mu_e\left(\nabla\times H^{+}\right)\times H^{+}\\ &= \mathrm{div}\bar{\mathbf{T}} + \mu_e\left[\left(H^{+}\cdot\nabla\right)H^{+} - \frac{\nabla H^{+^2}}{2}\right].\end{aligned} \tag{4}$$

Induction equation

$$\frac{\mathrm{d}H^{+}}{\mathrm{d}t} = \nabla\times\left(V\times H^{+}\right) + \frac{1}{\varsigma}\nabla^2 H^{+}\,. \tag{5}$$

$\varsigma = \sigma\mu_e$ denotes the magnetic diffusivity, σ the electrical conductivity, μ_e the magnetic permeability, ρ the density, $\mathrm{d}/\mathrm{d}t$ the material derivative, and $\mathbf{T}$ the Cauchy stress tensor. The Maxwell equations in the absence of displacement current are defined by

$$\nabla\cdot E = 0\,,\ \ \nabla\cdot H = 0\,, \tag{6}$$

$$\nabla\times E = -\mu_e\frac{\partial H}{\partial t}\,,\ \ \nabla\times H = J\,, \tag{7}$$

$$J = \sigma\left(E + \mu_e\left(V\times H\right)\right), \tag{8}$$

in which J, E, and H are the current density, the electric field, and the magnetic field, respectively. The Cauchy stress tensor $\mathbf{T}$ is given by

$$\mathbf{T} = -p\mathbf{I} + \mathbf{S}, \tag{9}$$

$$\begin{aligned}&\mathbf{S} + \bar{\lambda}_1\mathbf{S}^{\nabla} + \frac{1}{2}\left(\bar{\lambda}_1 - \bar{\mu}_1\right)\\ &\cdot\left(A_1\mathbf{S} + \mathbf{S}A_1\right) = \mu A_1\,,\end{aligned} \tag{10}$$

$$\mathbf{S}^{\nabla} = \frac{\mathrm{d}\mathbf{S}}{\mathrm{d}t} - \mathbf{S}L^{\mathrm{T}} - L\mathbf{S}, \tag{11}$$

$$L = \mathrm{grad}V,\ \ A_1 = L + L^{\mathrm{T}} \tag{12}$$

where $\mathbf{I}$, p, $\mathbf{S}$, μ, $\mathbf{S}^{\nabla}$, $\bar{\mu}_1$, and $\bar{\lambda}_1$, respectively, denote the identity tensor, the pressure, the extra stress tensor, the dynamic viscosity, the upper-convected derivative, and the relaxation times. The flow equations in the fixed frame become

$$\frac{\partial}{\partial \bar{R}}\{(R+R^*)V\}+R^*\frac{\partial U}{\partial X}=0, \tag{13}$$

$$\begin{aligned}&\rho\left[\frac{\partial V}{\partial t}+V\frac{\partial V}{\partial \bar{R}}+\frac{R^*U}{R^*+R}\frac{\partial V}{\partial X}-\frac{U^2}{R^*+R}\right]\\&=-\frac{\partial \bar{p}}{\partial \bar{R}}+\frac{1}{R^*+R}\frac{\partial}{\partial R}\left\{(R^*+\bar{R})\bar{S}_{RR}\right\}+\frac{R^*}{R^*+R}\\&\times\frac{\partial \bar{S}_{XR}}{\partial X}-\frac{\bar{S}_{XX}}{R+R^*}-\frac{\mu_e}{2\rho}\left(\frac{\partial H^{+2}}{\partial R}\right)+\frac{\mu_e}{\rho}\\&\times\left[\left(H_0\frac{R^*}{R^*+R}+\bar{h}_r\right)\frac{\partial \bar{h}_r}{\partial R}+\bar{h}_{\bar{x}}\frac{R^*}{R^*+R}\frac{\partial \bar{h}_r}{\partial X}-\frac{\bar{h}_x^2}{R^*+R}\right],\end{aligned} \tag{14}$$

$$\begin{aligned}&\rho\left[\frac{\partial U}{\partial t}+V\frac{\partial U}{\partial \bar{R}}+\frac{R^*U}{R^*+R}\frac{\partial U}{\partial X}+\frac{UV}{R^*+R}\right]\\&=-\frac{R^*}{R^*+R}\frac{\partial \bar{p}}{\partial X}+\frac{1}{(R^*+R)^2}\frac{\partial}{\partial R}\left\{(R^*+\bar{R})^2\bar{S}_{XR}\right\}\\&+\left(\frac{R^*}{R^*+R}\right)\frac{\partial \bar{S}_{XX}}{\partial X}-\frac{\mu_e}{2\rho}\frac{R^*}{R^*+R}\left(\frac{\partial H^{+2}}{\partial x}\right)\\&+\frac{\mu_e}{\rho}\left[\left(\frac{\bar{h}_x}{R^*+R}+\frac{\partial \bar{h}_x}{\partial R}\right)\left(H_0\frac{R^*}{R^*+R}+\bar{h}_r\right)\right.\\&\left.+\frac{R^*}{R^*+R}\bar{h}_{\bar{x}}\frac{\partial \bar{h}_x}{\partial X}\right].\end{aligned} \tag{15}$$

The above equations can be reduced in a wave frame $(r;x)$ by defining

$$\bar{x}=X-c\bar{t},\ \bar{r}=R,\ \bar{u}=U-c,\ \bar{v}=\bar{V}, \tag{16}$$

where (v,u) denote the velocity components in the wave frame. Now (13)–(15) give

$$\frac{\partial \bar{v}}{\partial \bar{r}}+\frac{R^*}{\bar{r}+R^*}\frac{\partial \bar{u}}{\partial \bar{x}}+\frac{\bar{v}}{\bar{r}+R^*}=0, \tag{17}$$

$$\begin{aligned}&\rho\left[-c\frac{\partial \bar{v}}{\partial \bar{x}}+\bar{v}\frac{\partial \bar{v}}{\partial \bar{r}}+\frac{R^*(\bar{u}+c)}{R^*+\bar{r}}\frac{\partial \bar{v}}{\partial \bar{x}}-\frac{(\bar{u}+c)^2}{R^*+\bar{r}}\right]\\&=-\frac{\partial \bar{p}}{\partial \bar{r}}+\frac{1}{R^*+\bar{r}}\frac{\partial}{\partial \bar{r}}\left\{(R^*+R)\bar{S}_{rr}\right\}+\left(\frac{R^*}{R^*+\bar{r}}\right)\frac{\partial \bar{S}_{xr}}{\partial \bar{x}}\\&-\frac{\bar{S}_{xx}}{\bar{r}+R^*}-\frac{\mu_e}{2}\left(\frac{\partial H^{+2}}{\partial \bar{r}}\right)+\mu_e\left[\left(H_0\frac{R^*}{R^*+\bar{r}}+\bar{h}_{\bar{r}}\right)\frac{\partial \bar{h}_{\bar{r}}}{\partial \bar{r}}\right.\\&\left.+\bar{h}_{\bar{x}}\frac{R^*}{R^*+\bar{r}}\frac{\partial \bar{h}_{\bar{r}}}{\partial \bar{x}}-\frac{\bar{h}_{\bar{x}}^2}{R^*+\bar{r}}\right],\end{aligned} \tag{18}$$

$$\begin{aligned}&\rho\left[-c\frac{\partial u}{\partial \bar{x}}+\bar{v}\frac{\partial \bar{u}}{\partial \bar{r}}+\frac{R^*(\bar{u}+c)}{R^*+\bar{r}}\frac{\partial \bar{u}}{\partial \bar{x}}-\frac{(\bar{u}+c)\bar{v}}{R^*+\bar{r}}\right]\\&=-\frac{R^*}{R^*+\bar{r}}\frac{\partial \bar{p}}{\partial \bar{x}}+\frac{1}{(R^*+\bar{r})^2}\frac{\partial}{\partial \bar{r}}\left\{(R^*+\bar{r})^2\bar{S}_{xr}\right\}\\&+\left(\frac{R^*}{R^*+\bar{r}}\right)\frac{\partial S_{xx}}{\partial \bar{x}}-\frac{\mu_e}{2\rho}\frac{R^*}{R^*+\bar{r}}\left(\frac{\partial H^{+2}}{\partial \bar{x}}\right)\\&+\mu_e\left[\left(\frac{\bar{h}_{\bar{x}}}{R^*+\bar{r}}+\frac{\partial \bar{h}_{\bar{x}}}{\partial \bar{r}}\right)\left(H_0\frac{R^*}{R^*+\bar{r}}+\bar{h}_{\bar{r}}\right)\right.\\&\left.+\frac{R^*}{R^*+\bar{r}}\bar{h}_{\bar{x}}\frac{\partial \bar{h}_{\bar{x}}}{\partial \bar{x}}\right],\end{aligned} \tag{19}$$

and the stress components through (2), (10)–(12), and (16) are given by

$$\begin{aligned}&\bar{S}_{rr}+\bar{\lambda}_1\left\{\left(-c\frac{\partial}{\partial \bar{x}}+v\frac{\partial \bar{v}}{\partial \bar{r}}+\frac{R^*}{R^*+\bar{r}}(\bar{u}+c)\frac{\partial}{\partial \bar{x}}\right)\bar{S}_{rr}-2\bar{S}_{rr}\right.\\&\left.\cdot\frac{\partial v}{\partial r}-\frac{2R^*}{R^*+\bar{r}}S_{rx}\right\}\frac{\partial v}{\partial x}+\frac{1}{2}\left(\bar{\lambda}_1-\bar{\mu}_1\right)\left\{4\bar{S}_{rr}\frac{\partial \bar{v}}{\partial \bar{r}}\right.\\&\left.+2\bar{S}_{rx}\left(\frac{\partial u}{\partial r}+\frac{R^*}{r+R^*}\frac{\partial v}{\partial x}-\frac{u+c}{r+R^*}\right)\right\}=2\mu\frac{\partial v}{\partial r},\end{aligned} \tag{20}$$

$$\begin{aligned}&\bar{S}_{rx}+\frac{1}{2}\left(\bar{\lambda}_1-\bar{\mu}_1\right)\left(\bar{S}_{rr}-\bar{S}_{rx}\right)\\&\cdot\left(\frac{\partial u}{\partial r}+\frac{R^*}{r+R^*}\frac{\partial v}{\partial x}-\frac{u+c}{r+R^*}\right)+\bar{\lambda}_1\\&\cdot\left\{\left(-c\frac{\partial}{\partial \bar{x}}+v\frac{\partial \bar{v}}{\partial \bar{r}}+\frac{R^*}{R^*+\bar{r}}(\bar{u}+c)\frac{\partial}{\partial \bar{x}}\right)\bar{S}_{rx}\right.\\&\left.-\bar{S}_{rr}\left(\frac{\partial u}{\partial r}-\frac{u+c}{r+R^*}\right)-\frac{R^*\bar{S}_{xx}}{r+R^*}\frac{\partial v}{\partial x}\right\}\\&=\bar{\mu}\left(\frac{\partial u}{\partial r}+\frac{R^*}{r+R^*}\frac{\partial v}{\partial x}-\frac{u+c}{r+R^*}\right),\end{aligned} \tag{21}$$

$$\begin{aligned}&\bar{S}_{xx}+\frac{1}{2}\left(\bar{\lambda}_1-\bar{\mu}_1\right)\left\{2\bar{S}_{rx}\left(\frac{\partial u}{\partial r}+\frac{R^*}{r+R^*}\frac{\partial v}{\partial x}-\frac{u+c}{r+R^*}\right)\right.\\&\left.+4S_{xx}\left(\frac{v}{r+R^*}+\frac{R^*}{R^*+\bar{r}}\frac{\partial u}{\partial x}\right)\right\}+\bar{\lambda}_1\left\{\left(-c\frac{\partial}{\partial \bar{x}}\right.\right.\\&\left.\left.+v\frac{\partial \bar{v}}{\partial \bar{r}}+\frac{R^*}{R^*+\bar{r}}(\bar{u}+c)\frac{\partial}{\partial \bar{x}}\right)S_{xx}-2\bar{S}_{rx}\right.\\&\left.\times\left(\frac{\partial u}{\partial r}-\frac{u+c}{r+R^*}\right)-2S_{xx}\left(\frac{v}{r+R^*}+\frac{R^*}{R^*+\bar{r}}\frac{\partial u}{\partial x}\right)\right\}\\&=\bar{\mu}\left(\frac{v}{r+R^*}+\frac{R^*}{r+R^*}\frac{\partial u}{\partial x}\right),\end{aligned} \tag{22}$$

To facilitate the analysis, we use the following dimensionless variables:

$$
\begin{aligned}
&x=\frac{\bar{x}}{\lambda},\ r=\frac{\bar{r}}{a},\ t=\frac{c\bar{t}}{\lambda},\ p=\frac{a^2\bar{p}}{c\lambda\mu},\ M^2=\mathrm{Re}S^2R_{\mathrm{m}},\\
&S_{ij}=\frac{a\bar{S}_{ij}}{c\mu},\ \delta=\frac{a}{\lambda},\ u=\frac{\bar{u}}{c},\ v=\frac{\bar{v}}{c},\ k=\frac{R^*}{a},\\
&E=\frac{-\bar{E}}{cH_0\mu_e},\ \lambda_1=\frac{\bar{\lambda}_1c}{a},\ \mathrm{Re}=\frac{ca\rho}{\mu},\ \mathrm{R_m}=\sigma\mu_eac,\\
&S=\frac{H_0}{c}\sqrt{\frac{\mu_e}{\rho}},\ \phi=\frac{\bar{\phi}}{H_0a},\ \mu_1=\frac{\bar{\mu}_1c}{a},\ \bar{h}_{\bar{x}}=-\bar{\phi}_{\bar{r}},\\
&\bar{h}_{\bar{r}}=\frac{R^*}{R^*+\bar{r}}\bar{\phi}_{\bar{x}},\ p_{\mathrm{m}}=p+\frac{1}{2}\mathrm{Re}\delta\frac{\mu_e\left(H^+\right)^2}{\rho c^2},
\end{aligned}
\tag{23}
$$

where δ, Re, R_{m}, S, and M are the wave, Reynolds, magnetic Reynolds, Stommer, and Hartman numbers, respectively. The total pressure p_{m} is a sum of ordinary and magnetic pressures, E the electric field strength, ϕ the magnetic force function, λ_1 and μ_1 the relaxation times, and S_{xr}, S_{rr}, and S_{xx} are the components of an extra stress tensor $\mathbf{S}$.

Defining the stream function ψ and the magnetic force ϕ function by

$$
\begin{aligned}
&u=-\frac{\partial\psi}{\partial r},\ v=\delta\frac{k}{k+r}\frac{\partial\psi}{\partial x},\\
&h_x=-\frac{\partial\phi}{\partial r},\ h_r=\delta\frac{k}{k+r}\frac{\partial\phi}{\partial x},
\end{aligned}
\tag{24}
$$

we see that (17) is satisfied identically; under long wavelength and low Reynolds number approach, one has

$$
\frac{\partial p}{\partial r}=0, \tag{25}
$$

$$
\begin{aligned}
\frac{\partial p}{\partial x}=&\frac{1}{k(k+r)}\frac{\partial}{\partial r}\left[(k+r)^2S_{rx}\right]\\
&+\mathrm{Re}S^2\left[\frac{1}{k+r}\frac{\partial\phi}{\partial r}+\frac{\partial^2\phi}{\partial r^2}\right],
\end{aligned}
\tag{26}
$$

$$
E=\frac{k}{k+r}\frac{\partial\psi}{\partial r}+\frac{1}{\mathrm{R_m}}\left[\frac{\partial^2\phi}{\partial r^2}+\frac{1}{k+r}\frac{\partial\phi}{\partial r}\right], \tag{27}
$$

$$
\begin{aligned}
S_{rx}=&-\frac{\partial^2\psi}{\partial r^2}-\frac{1}{k+r}\left(1-\frac{\partial\psi}{\partial r}\right)\\
&\cdot\left[1-\xi\left(-\frac{\partial^2\psi}{\partial r^2}-\frac{1}{k+r}\right.\right.\\
&\left.\left.\cdot\left(1-\frac{\partial\psi}{\partial r}\right)\right)^2\right]^{-1},
\end{aligned}
\tag{28}
$$

where $\xi=\left(\lambda_1^2-\mu_1^2\right)$ is the pseudoplastic fluid parameter, and (25) shows that $p\neq p(r)$.

The dimensionless boundary conditions for the present problem are

$$
\begin{aligned}
&\Psi=-\frac{F}{2},\ \frac{\partial\Psi}{\partial r}=1,\ \phi=0\ \text{ at }\ y=h,\\
&\Psi=\frac{F}{2},\ \frac{\partial\Psi}{\partial r}=1,\ \phi=0\ \text{ at }\ y=-h.
\end{aligned}
\tag{29}
$$

Here the dimensionless time mean flow rate F in the wave frame is related to the dimensionless time mean flow rate θ in the laboratory frame as

$$
\theta=F+2,\ F=-\int_{-h}^{h}\frac{\partial\Psi}{\partial r}\,\mathrm{d}r. \tag{30}
$$

3. Solution Methodology

With an interest in the series solution, we expand the following quantities in the parameter as follows:

$$
\Psi=\Psi_0+\xi\Psi_1+O(\xi)^2, \tag{31}
$$

$$
F=F_0+\xi F_1+O(\xi)^2, \tag{32}
$$

$$
p=p_0+\xi p_1+O(\xi)^2, \tag{33}
$$

$$
\phi=\phi_0+\xi\phi_1+O(\xi)^2, \tag{34}
$$

$$
S_{rx}=S_{0rx}+\xi S_{1rx}+O(\xi)^2. \tag{35}
$$

The corresponding zeroth and first-order systems are presented in the subsequent subsections.

3.1. Zeroth-Order System

$$
\begin{aligned}
&\frac{\partial p_0}{\partial x}=\frac{1}{k(r+k)}\frac{\partial}{\partial r}\left\{(r+k)^2S_{0rx}\right\}\\
&\qquad+M^2\left(E-\frac{k}{r+k}\frac{\partial\psi_0}{\partial r}\right),\\
&\frac{\partial}{\partial r}\left[\frac{1}{k(r+k)}\frac{\partial}{\partial r}\left\{(r+k)^2S_{0rx}\right\}\right]\\
&+M^2k^2\frac{\partial}{\partial r}\left(-\frac{1}{r+k}\frac{\partial\psi_0}{\partial r}\right)=0,\\
&\frac{\partial^2\phi_0}{\partial r^2}+\frac{1}{r+k}\frac{\partial\phi_0}{\partial r}=\mathrm{R_m}\left(E-\frac{k}{k+r}\frac{\partial\psi_0}{\partial r}\right),\\
&S_{0rx}=-\frac{\partial^2\psi_0}{\partial r^2}-\frac{1}{k+r}\left(1-\frac{\partial\psi_0}{\partial r}\right),\\
&\Psi_0=-\frac{F_0}{2},\ \frac{\partial\Psi_0}{\partial r}=1,\ \phi_0=0\ \text{ at }\ y=h,\\
&\Psi_0=\frac{F_0}{2},\ \frac{\partial\Psi_0}{\partial r}=1,\ \phi_0=0\ \text{ at }\ y=-h.
\end{aligned}
\tag{36}
$$

3.2. First-Order System

$$\begin{aligned}
&\frac{\partial p_1}{\partial x} = \frac{1}{k(r+k)}\frac{\partial}{\partial r}\left\{(r+k)^2 S_{1rx}\right\} \\
&\qquad + M^2\left(-\frac{k}{r+k}\frac{\partial \psi_1}{\partial y}\right), \\
&\frac{\partial}{\partial r}\left[\frac{1}{k(r+k)}\frac{\partial}{\partial r}\left\{(r+k)^2 S_{1rx}\right\}\right] \\
&+ M^2 k^2 \frac{\partial}{\partial r}\left(-\frac{1}{r+k}\frac{\partial \psi_1}{\partial r}\right) = 0, \\
&\frac{\partial^2 \phi_1}{\partial y^2}\frac{1}{r+k}\frac{\partial \phi_1}{\partial r} = -\frac{\mathrm{R_m} k}{k+r}\frac{\partial \psi_1}{\partial r}, \\
&S_{1rx} = -\frac{\partial^2 \psi_1}{\partial r^2} - \frac{1}{k+r}\frac{\partial \psi_1}{\partial r} \\
&\qquad - \left[-\frac{\partial^2 \psi_0}{\partial r^2} + \frac{1}{k+r}\left(\frac{\partial \psi_0}{\partial r} - 1\right)\right]^3, \\
&\Psi_1 = -\frac{F_1}{2}, \ \frac{\partial \Psi_1}{\partial r} = 0, \ \phi_1 = 0 \ \text{at} \ y = h, \\
&\Psi_1 = \frac{F_1}{2}, \ \frac{\partial \Psi_1}{\partial r} = 0, \ \phi_1 = 0 \ \text{at} \ y = -h.
\end{aligned} \tag{37}$$

The solution of above systems with

$$F_0 = F - \xi F_1 \tag{38}$$

yields the results given below.

$$\begin{aligned}
&\psi(r) = C_1 + C_2(r+k)^2 + (r+k)(C_3\cos(b\ln(r+k)) \\
&+ C_4\sin(b\ln(r+k))) - \frac{r+k}{b^2} + \xi\left[A_1 + A_2(r+k)^2\right. \\
&+ (r+k)\left(A_3\cos(b\ln(r+k)) + A_4\sin(b\ln(r+k))\right) \\
&- \frac{1}{r+k}\left\{L_0 + L_1\ln(r+k)\sin(b\ln(r+k))\right. \\
&+ L_2\ln(r+k)\cos(b\ln(r+k)) + L_3\cos(3b\ln(r+k)) \\
&\left.\left. + L_4\sin(3b\ln(r+k)) + L_5\cos(2b\ln(r+k))\right\}\right. \\
&\left. \cdot \frac{1}{r+k}L_6\sin(2b\ln(r+k))\right],
\end{aligned} \tag{39}$$

$$\begin{aligned}
&\phi(r) = B_1 + B_2\ln(r+k) - \frac{1}{4}\mathrm{R_m}\xi L_0(\ln(r+k))^2 + \frac{1}{4}\mathrm{R_m} \\
&\cdot\left(E + \frac{1+\xi}{b^2}\right)L_0(r+k)^2 - \frac{2\mathrm{R_m}}{4b^2}(C_2 + \xi A_2)(r+k)^3 \\
&- \frac{L_1\xi\mathrm{R_m}}{b^2}\sin(b\ln(r+k)) - \cos(b\ln(r+k)) \times \frac{L_1\xi\mathrm{R_m}}{b^2} \\
&+ \frac{\xi\mathrm{R_m}}{4b^2}(2bL_5 + L_6)\sin(2b\ln(r+k)) + \frac{\xi\mathrm{R_m}}{4b^2}(-2bL_6 \\
&+ L_5) \times \cos(2b\ln(r+k)) + \frac{\xi\mathrm{R_m}}{9b^2}(3bL_3 + L_4)\sin(3b \\
&\cdot\ln(r+k)) + \frac{\xi\mathrm{R_m}}{9b^2}(-3bL_3 + L_4)\cos(3b\ln(r+k)) \\
&+ \frac{\xi\mathrm{R_m}}{b^2}(bL_1 - L_2)\Big(-\ln(r+k)\cos(3b\ln(r+k)) + \frac{2}{b} \\
&\cdot\sin(b\ln(r+k))\Big) + \Big(\ln(r+k)\sin(b\ln(r+k)) + \frac{2}{b} \\
&\cdot\cos(b\ln(r+k))\Big)(L_1 + bL_2) - \frac{\mathrm{R_m}(r+k)^2}{b^4 + 8b^2 + 16} \\
&\cdot\left((4-b^2)\cos(b\ln(r+k)) + \frac{4}{b}\sin(b\ln(r+k))\right) \\
&\cdot(C_3 + bC_4 + \xi(A_3 + bA_4)) - \frac{\mathrm{R_m}(r+k)^2}{b^4 + 8b^2 + 16} \\
&\cdot(C_4 - bC_3 + \xi(A_4 - bA_3)) \\
&\cdot\left((4-b^2)\sin(b\ln(r+k)) - \frac{4}{b}\cos(b\ln(r+k))\right),
\end{aligned} \tag{40}$$

with

$$\begin{aligned}
&b = \sqrt{k^2M^2 - 1}, \ L_0 = \frac{21l_1}{3(b^2+4)}, \\
&L_1 = \frac{21l_2 - b^2l_2 - 10bl_3}{2b^3(b^2+1)}, \ L_2 = \frac{21l_3 - b^2l_3 + 10bl_2}{2b^3(b^2+1)}, \\
&L_3 = \frac{21l_4 - 9b^2l_4 - 30bl_5}{8b^2(9b^2+1)}, \ L_4 = \frac{21l_5 - 9b^2l_5 + 30bl_4}{8b^2(9b^2+1)}, \\
&L_5 = \frac{21l_6 - 4b^2l_6 - 20bl_7}{3b^2(4b^2+1)}, \ L_6 = \frac{21l_7 - 4b^2l_7 + 20bl_6}{3b^2(4b^2+1)}, \\
&l_1 = (1+b^2)^3\left(\frac{1}{b^6} + \frac{3\left(C_3^2 + C_4^2\right)}{b^2}\right), \\
&l_2 = -(1+b^2)^3\left(\frac{3C_3^3}{4} + \frac{3C_3}{b^4} + \frac{3C_3C_4^2}{4}\right), \\
&l_3 = -(1+b^2)^3\left(\frac{3C_4^3}{4} + \frac{3C_4}{b^4} + \frac{3C_4C_3^2}{4}\right), \\
&l_4 = -\frac{1}{4}(1+b^2)^3\left(C_3^3 - 3C_3C_4^2\right)^2, \\
&l_5 = \frac{(1+b^2)^3}{4}\left(C_3^3 - 3C_3^2C_4\right), \\
&l_6 = \frac{3(1+b^2)^3}{b^2}\left(C_3^2 - C_4^2\right), \ l_7 = \frac{3(1+b^2)^3C_3C_4}{b^2}.
\end{aligned}$$

Note that C_i $(i = 1-4)$, A_i $(i = 1-4)$, B_i $(i = 1,2)$ can be determined by the boundary conditions (37) in (39)–(40). Clearly, once the stream function and

the magnetic force function are determined, the other physical quantities of interest can also be computed. Thus the pressure gradient $\mathrm{d}p/\mathrm{d}x$, axial induced magnetic field h_x, current density J_z, and pressure rise ΔP_λ are defined as

$$\frac{\mathrm{d}p}{\mathrm{d}x} = -\frac{\partial}{\partial r}\left[(k+r)^2\left(-\frac{\partial^2\psi}{\partial r^2} - \frac{1}{k+r}\left(1-\frac{\partial\psi}{\partial r}\right) - \xi\left[\frac{\partial^2\psi}{\partial r^2} + \frac{1}{k+r}\left(1-\frac{\partial\psi}{\partial r}\right)\right]^3\right)\right] \times \frac{1}{k(k+r)} + M^2\left[E - \frac{k}{k+r}\frac{\partial\psi}{\partial r}\right], \tag{41}$$

$$h_x = -\frac{\partial\phi}{\partial r}, \tag{42}$$

$$J_z = -\frac{\partial^2\phi}{\partial r^2}, \tag{43}$$

$$\Delta P_\lambda = \int_0^1 \left(\frac{\mathrm{d}p}{\mathrm{d}x}\right)_{r=0} \mathrm{d}x. \tag{44}$$

4. Results and Discussion

This section presents the results for pressure rise per wavelength ΔP_λ, velocity u, axial induced magnetic field h_x, and current density J_Z through the influence of curvature parameter k, pseudoplastic fluid parameter ξ, Hartman number M, and magnetic Reynolds number R_m. Interestingly, k controls the magnitude of curvature. Results for rectangular straight channel are deduced for larger values of k (say $k \to \infty$). The effects of emerging parameters are plotted in Figures 2–7.

The analysis of peristaltic pumping is important when the moving wall induces a curvilinear fluid motion. The pumping action is due to the dynamic pressure exerted by the walls on the fluid trapped between the contraction regions. The effect of curvature parameter k on the pressure rise is discussed in Figure 2a. We observe that the presence of curvature increases ΔP_λ in the pumping region [41]. Pressure rise increases as one moves from curved to straight channel. The peristalsis has to work against lesser pressure rise in a curved channel in comparison to a straight channel. The free pumping flux increases in going from curved to straight channels. In the copumping region, where the pressure assists the flow, a mixed behaviour of the curvature parameter is observed for fixed values of flow rate. The influence of ξ on the pressure rise per wavelength is shown in Figure 2b. In the pumping region ($\Delta p_\lambda > 0$, $\theta > 0$), Δp increases by increasing parameter ξ for fixed flow rate θ. This means that the peristalsis has to work against a greater pressure rise for a pseudoplastic fluid than for a viscous fluid in the pumping region. For free pumping

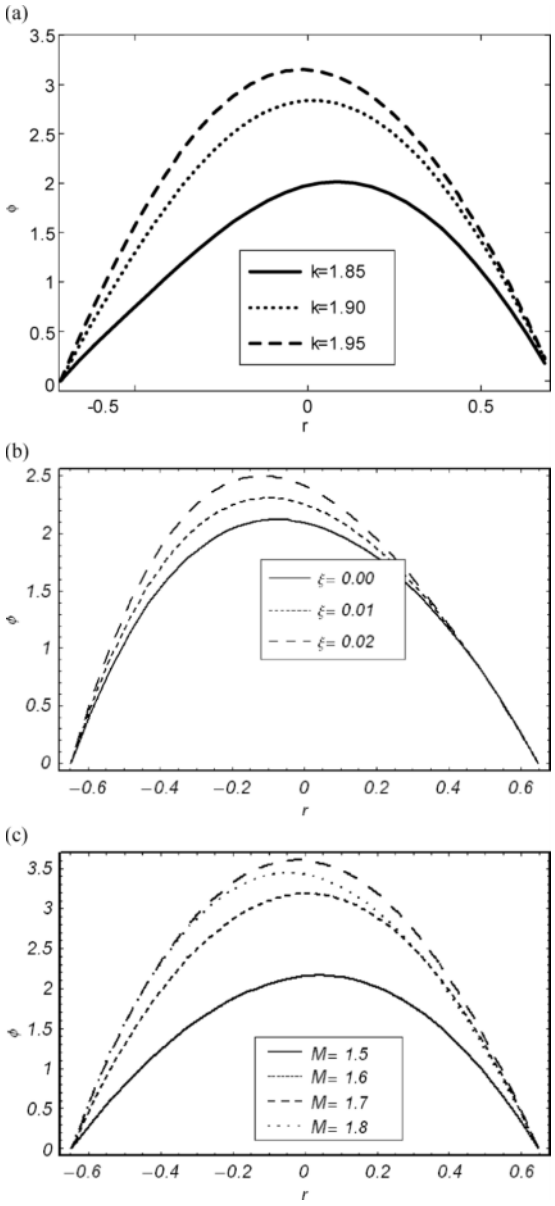

Fig. 4. (a) Magnetic force function ϕ versus r for $\xi = 0.01$, $M = 2$, $\alpha = 0.3$, $E = 0$, $x = -0.2$, $R_\mathrm{m} = 4$, and $\theta = -3$. (b) Magnetic force function ϕ versus r for $M = 2$, $\alpha = 0.6$, $k = 2$, $E = -1$, $x = 0.6$, $R_\mathrm{m} = 4$, and $\theta = 2.8$. (c) Magnetic force function ϕ versus r for $\xi = 0.01$, $\alpha = 0.6$, $k = 2$, $E = -1$, $x = 0.6$, $R_\mathrm{m} = 4$, and $\theta = 2.8$.

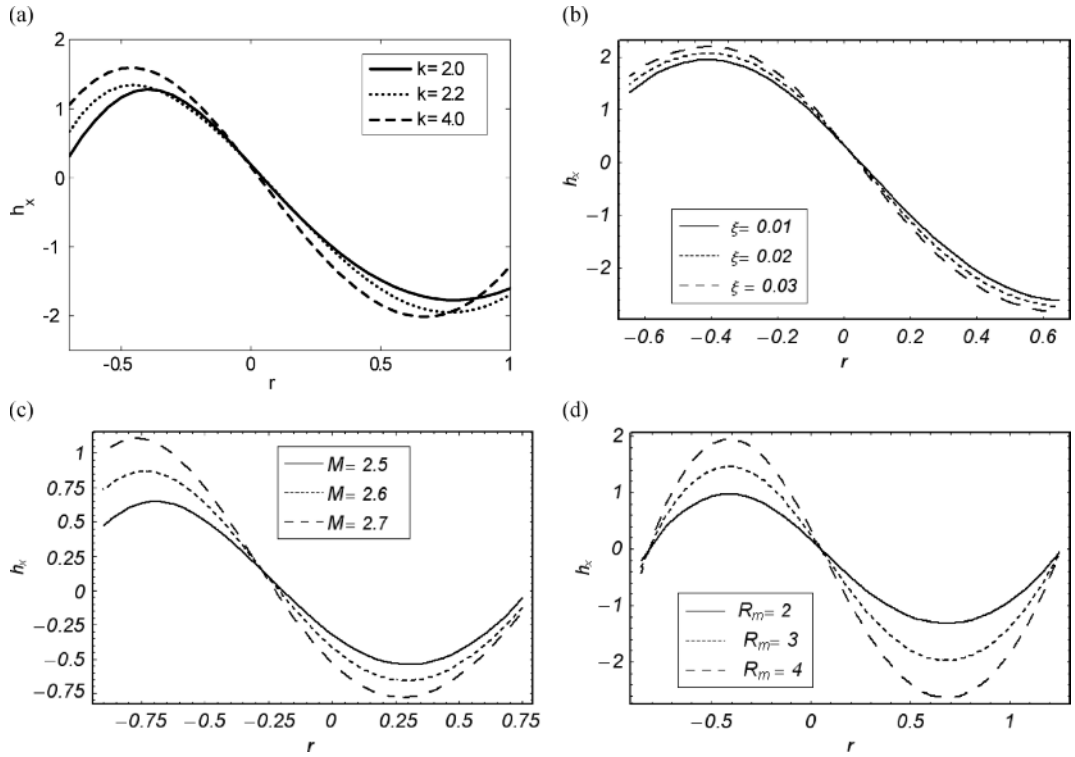

Fig. 5. (a) Axial induced magnetic field h_x versus r for $\xi = 0.01$, $\alpha = 0.6$, $M = 2.3$, $E = 1$, $R_{\rm m} = 3$, $x = 0.6$, $\theta = 2.8$. (b) Axial induced magnetic field h_x versus r for $\alpha = 0.6$, $M = 2.3$, $E = 1$, $k = 3.5$, $R_{\rm m} = 3$, $x = 0.6$, and $\theta = 2.8$. (c) Axial induced magnetic field h_x versus r for $\xi = 0.01$, $\alpha = 0.1$, $R_{\rm m} = 4$, $L = 1$, $k = 3.5$, $x = -0.2$, and $\theta = 1$. (d) Axial induced magnetic field h_x versus r for $\xi = 0.01$, $\alpha = 0.6$, $M = 2.3$, $L = 1$, $k = 2$, $x = 0.6$ and $\theta = 2.8$.

and copumping regions, it is noted that Δp decreases by increasing ξ. Figure 2c describes the pressure rise Δp_λ against the mean flow rate θ for different values of M. The Hartman number M is a dimensionless quantity characterizing the flow of a conducting fluid in a transverse magnetic field. Here an increase in M investigated a decrease in the pressure rise. We observe that ΔP_λ in the pumping region ($\Delta p_\lambda > 0$, $\theta > 0$) decreases by increasing M for the fixed values of flow rate. However for the case of copumping ($\Delta p_\lambda < 0$), the flow rate θ is an increasing function of M. There is no difference between the pseudoplastic fluid and the viscous fluid in the free pumping region ($\Delta p_\lambda = 0$). A deviation in the behaviour of Hartman number M on ΔP_λ is observed because of the incorporation of curvature effects. Clearly, the results for a planar channel are deduced when k is large [41].

In Figure 3a, the axial velocity u is plotted for various values of curvature parameter k. The position of the maximum in the profiles is a function of k [41]. Moreover, the profiles are not symmetric about $r = 0$. A shift of the profiles for smaller values of k (i. e., an increase in the curvature of channel) towards the lower wall is noticed, and symmetry occurs for $k \to \infty$. The variation in axial velocity for the pseudoplastic fluid parameter is presented in Figure 3b. Here ξ is the material parameter which physically measures the elastic and viscous effects on the fluid flow. It is revealed that the maximum in $u(r)$ for the Newtonian fluid ($\xi = 0$) lies below the maximum in $u(r)$ for the pseudoplastic fluid ($\xi \neq 0$). Thus we see that the velocity in the pseudoplastic fluid is larger compared with the Newtonian fluid. The difference in velocity between Newtonian and non-Newtonian fluids also holds for bigger parameter space. Since the graphical visibility was seen for smaller values ($\xi = 0.00, 0.005, 0.010$), so we plotted $u(r)$ for narrow interval of ξ parameter values. The axial velocity distribution u for different values of Hartman number M is shown in Figure 3c. It is found that the velocity profile is not symmetric about the central line of the channel due to the channel curvature.

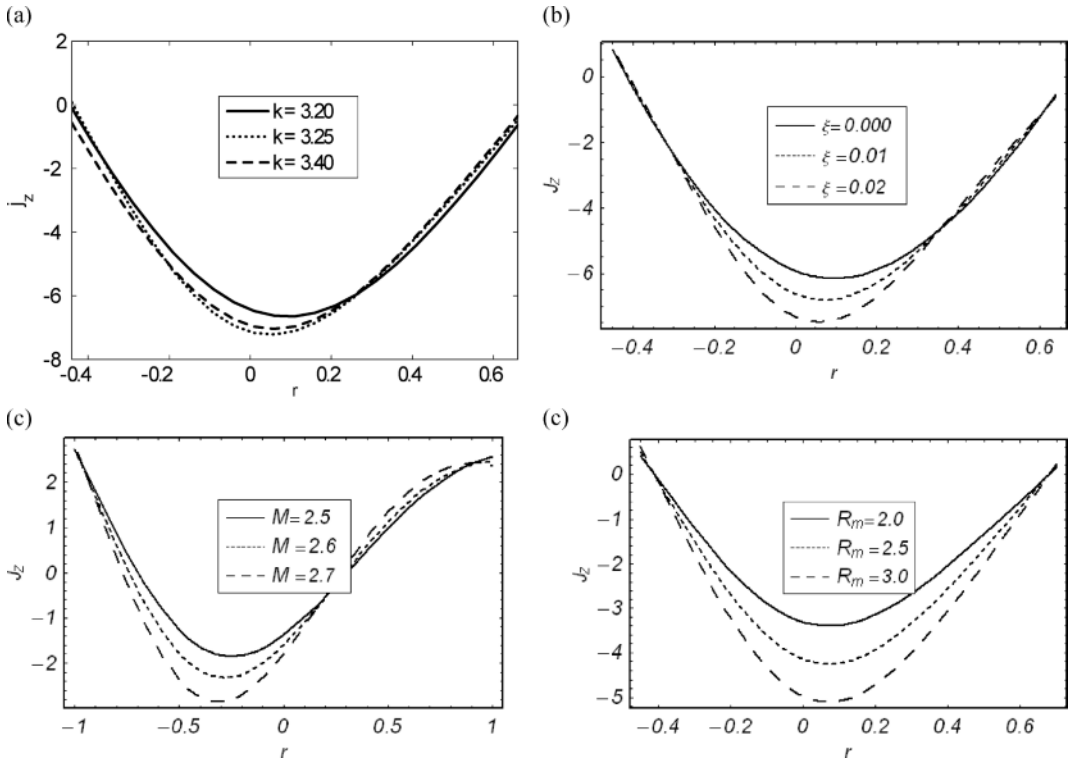

Fig. 6. (a) Current density versus J_z versus r for $\alpha = 0.6$, $\xi = 0.01$, $R_{\mathrm{m}} = 4$, $M = 2.4$, $x = 0.6$, $E = 1$, and $\theta = 2.8$. (b) Current density J_z versus r for $\alpha = 0.6$, $R_{\mathrm{m}} = 4$, $M = 2.3$, $k = 3.5$, $x = 0.6$, $E = 1$, and $\theta = 2.8$. (c) Current density J_z versus r for $\alpha = 0.1$, $\xi = 0.01$, $R_{\mathrm{m}} = 4$, $k = 3.5$, $x = -0.2$, $E = 1$, and $\theta = 1.5$. (d) Current density J_z versus r for $\alpha = 0.6$, $\beta = 0.01$, $k = 3.5$, $M = 2.3$, $x = 0.6$, $E = 1$, and $\theta = 2.8$.

The behaviour of M near the walls of the channel is quite opposite to that of the centre of the channel. The magnitude of velocity is a decreasing function of M at $r = 0$.

The motion of a conductive fluid across the magnetic field generates currents, which thereby affect the propagating field. On the other hand, the flow of an electric current across a magnetic field is associated with a body force, the so called Lorentz force, which influences the fluid flow. To investigate the effects of magnetic field characteristics under the influence of k, ξ, and M, we plotted Figures 4a–c. It is shown that the parabolic profiles for the magnetic force function depict a left shift at $r = 0$. The magnetic force function is zero at the walls, which is in accordance with the imposed boundary conditions. These profiles are increasing functions of k, ξ, and M near the upper wall of the channel.

Figures 5a–d discuss the variation of axial induced magnetic field h_x against r for different values of k, ξ, M, and R_{m}. In the half region, the induced magnetic field is in one direction whereas in the other half it is in the opposite direction [38]. It is evident here that the magnitude of h_x increases with k, ξ, M, and R_{m}. The current density distribution J_z for different values of k, ξ, M, and R_{m} is plotted in Figures 6a–c. These plots indicate that the curves of J_z are parabolic in nature and the magnitude of the current density J_z increases at the centre of the channel while it decreases near the walls by increasing k, ξ, and M. A shift in the profiles is observed towards the lower wall. For larger values of k, symmetry in the profiles is attained, and the obtained results are compatible with existing studies [34–36]. Physically, the balance of magnetic advection and magnetic diffusion is described by the magnetic Reynolds number. We see that R_{m} has an increasing effect on the current density distribution (Fig. 5d).

Streamlines represent the trajectories of fluid particles in a flow. The formation of an internally circulating bolus of fluid by the closed streamlines is known as trapping. The streamlines are shown in order to de-

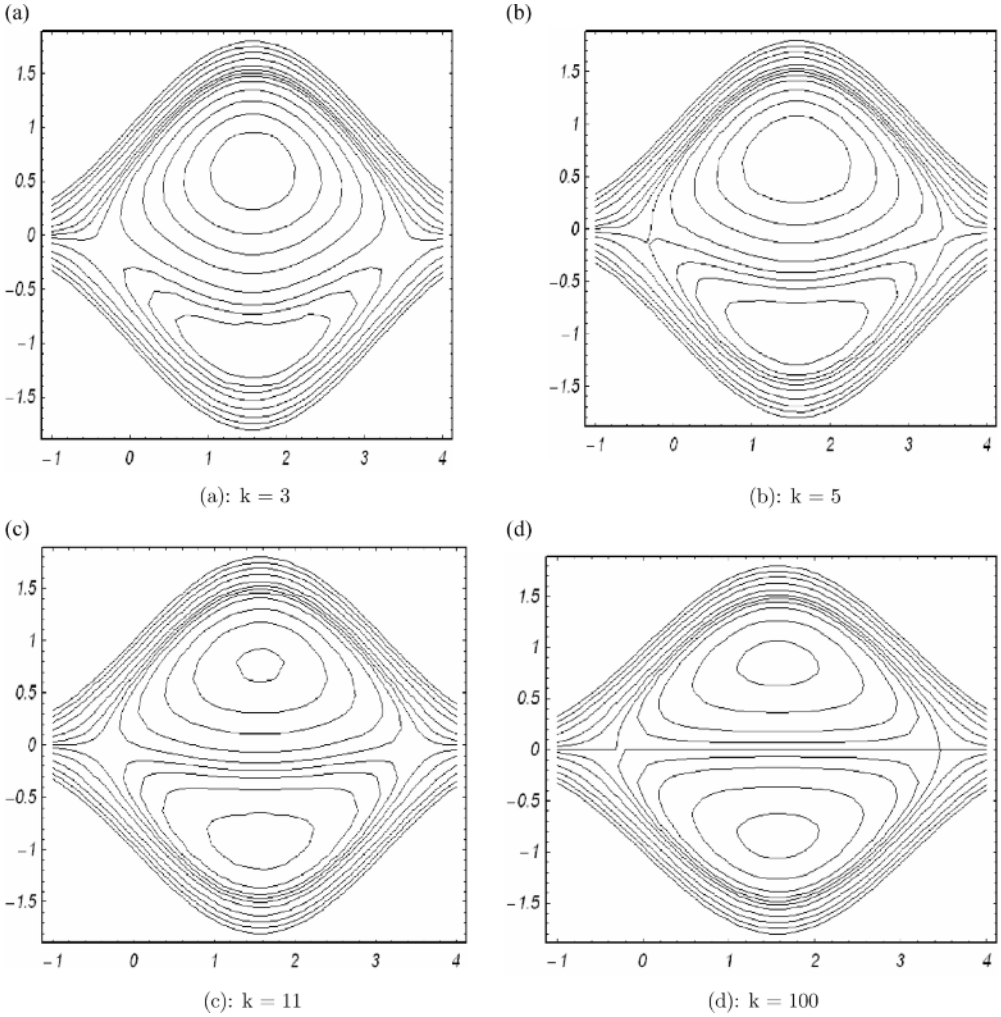

Fig. 7. Stream lines for different values of k.

pict the variations of k on the trapping. The circulating bolus attains symmetry about $r = 0$ for large values of k. (Figs. 7a – d).

5. Concluding Remarks

The effects of curvature and induced magnetic field on the peristaltic flow of a pseudoplastic fluid are explored; magnetic field characteristics are particularly emphasized. The main points are given below.

- The absolute axial velocity in a pseudoplastic fluid is larger than in a Newtonian fluid.
- The pressure rise per wavelength for a pseudoplastic fluid is larger than for a viscous fluid.
- The tilt in the velocity profiles shows that the flow is more towards the lower wall.
- The magnitude of induced magnetic field and current density in a non-Newtonian fluid is much larger compared with a viscous fluid.
- The symmetry of flow quantities such as velocity, current density, and induced magnetic field at $r = 0$ is disturbed due to the curvature. When $k \to \infty$, the results for a planar channel are recovered.

Acknowledgement

The research of Dr. Alsaedi was partially supported by Deanship of scientific Research (DSR) King Abdul Aziz University Jeddah, Saudi Arabia.

[1] T. W. Latham, MS Thesis, MIT Cambridge MA, Massachusetts 1966.
[2] D. Tripathi, J. Fluid Eng. ASME **133**, 121104 (2011).
[3] D. Tripathi, Int. J. Therm. Sci. **51**, 91 (2012).
[4] D. Tripathi, J. Bion. Eng. **9**, 119 (2012).
[5] D. Tripathi, Transp. Por. Media **92**, 559 (2012).
[6] S. K. Pandey and M. K. Chaube, Math. Comp. Model. **52**, 501 (2010).
[7] S. K. Pandey and D. Tripathi, Appl. Math. Mech.-Engl. Ed. **33**, 15 (2012).
[8] S. Srinivas and M. Kothandapani, Int. Commun. Heat Mass Transf. **35**, 514 (2008).
[9] Y. Abd elmaboud, Kh. S. Mekheimer, Appl. Math. Model. **35**, 2695 (2011).
[10] T. Hayat, S. Noreen, M. S. Alhothuali, S. Asghar, and A. Alhomaidan, Int. J. Heat Mass Tranf. **55**, 443 (2012).
[11] T. Hayat, S. Hina, and N. Ali, Commun. Nonlin. Sci. Numer. Simul. **15**, 1526 (2010).
[12] Kh. S. Mekheimer and Y. Abd elmaboud, Phys. Lett A **372**, 1657 (2008).
[13] Kh. S. Mekheimer, S. Z.-A. Husseny, and A. I. Abd el Lateef, Appl. Bion. Biomech. **8**, 295 (2011).
[14] Y. Abd elmaboud and Kh. S. Mekheimer, Appl. Math. Model. **35**, 2695 (2011).
[15] Z. M. Gharsseldien, Kh. S. Mekheimer, and A. S. Awad, J. Appl. Bion. Biomech. **7**, 95 (2010).
[16] D. Tripathi and O. A. Bég, Transp. Porous Media, doi:10.1007/s11242-012-0046-5 (2012).
[17] D. Tripathi, S. K. Pandey, A. Siddiqui, and O. A. Bég, Comp. Meth. Biomech. Biomed. Eng., doi:10.1080/10255842.2012.703660 (2012).
[18] D. Tripathi, S. K. Pandey, and S. Das, Appl. Math. Comput. **215**, 3645 (2010).
[19] D. Tripathi, S. K. Pandey, A. Siddiqui, and O. A. Beg, Comp. Meth. Biomech. Biomed. Eng. doi:10.1080/10255842.2012.688109 (2012).
[20] O. A. Bég, Proc. Inst. Mech. Eng. H: J. Eng. Med. **226**, 631 (2012).
[21] S. Nadeem, N. S. Akbar, T. Hayat, and A. A. Hendi, Appl. Math. Comput. **217**, 7108 (2011).
[22] S. Nadeem and M. Awais, J. Porous Media **13**, 973 (2010).
[23] T. Hayat, N. Ahmad, and N. Ali, Commun. Nonlin. Sci. Numer. Simul. **13**, 1581 (2008).
[24] T. Hayat, N. Saleem, and S. Mesloub, Z. Naturforsch. **66a**, 215 (2011).
[25] T. Hayat, Z. Asghar, S. Asghar, and S. Mesloub, J. Tiawan Instit. Chem. Eng. **41**, 553 (2010).
[26] S. K. Pandey and M. K. Chaube, Commun. Nonlin. Sci. Numer. Simul. **16**, 3591 (2011).
[27] N. T. M. Eldabe, M. F. Al-Sayad, A. Y. Galy, and H. M. Sayed, Physica A **383**, 253 (2007).
[28] T. Hayat, M. Khan, A. M. Siddiqui, and S. Asghar, Commun. Nonlin. Sci. Numer. Simul. **12**, 910 (2007).
[29] M. Kothandapani and S. Srinivas, Int. J. Nonlin. Mech. **43**, 915 (2008).
[30] Y. Abd elmaboud, Commun. Nonlin. Sci. Numer. Simul. **17**, 685 (2012).
[31] S. Srinivas and R. Muthuraj, Math. Comput. Modell. **54**, 1213 (2011).
[32] T. Hayat and O. U. Mehmood, Commun. Nonlin. Sci. Numer. Simul. **16**, 1363 (2011).
[33] K. B. Pavlov and V. I. Vishnyakov, Translated from Magnitnaya Gidrodinamika. **8**, 174 (1972).
[34] Kh. S. Mekheimer, Phys. Lett. A **372**, 4271 (2008).
[35] T. Hayat, Y. Khan, N. Ali, and Kh. S. Mekheimer, Numer. Meth. Partial Diff. Eqs. **26**, 346 (2010).
[36] T. Hayat, N. Saleem, and N. Ali, Commun. Nonlin. Sci. Numer. Simul. **15**, 2407 (2010).
[37] T. Hayat and S. Noreen, C. R Mécanique **338**, 518 (2010).
[38] Kh. S. Mekheimer, J. Appl. Math. **2008**, 570825 (2008).
[39] H. Sato, T. Kawai, T. Fujita, and M. Okabe, Trans. The Japan Soc. Mech. Engs. B **66**, 679 (2000).
[40] N. Ali, M. Sajid, and T. Hayat, Z. Naturforsch. **65a**, 191 (2010).
[41] N. Ali, M. Sajid, T. Javed, and Z. Abbas, Europ. J. Mech. B/Fluids **29**, 387 (2010).
[42] N. Ali, M. Sajid, T. Javed, and Z. Abbas, Chin. Phys. Lett. **28**, 14704 (2011).